Segmentation of the Left Ventricle in SPECT by an Active Surface

Clemens M. Hentschke*, Karin Engel, Sebastian Schäfer, and Klaus D. Tönnies

Department of Simulation and Graphics, Otto-von-Guericke-University Magdeburg, Germany

Abstract. We present a method for the semi-automatic, model-driven segmentation of the Left Ventricle (LV) in cardiac SPECT data. Accurate segmentation of the LV allows computation of quantities that describe the degree of a perfusion defect. A 3D surface is initialised in the dataset and deforms to fit the shape of the LV. The model is chosen from a small number of prototypes. The behaviour of the dynamic model is controlled by an Active Surface which is simulated by using the Finite Element Method. Segmentation results were obtained for nine datasets for which a manual segmentation by an expert existed. Results show a good agreement with the manual segmentation with an average of the mean contour distance of 0.24 voxel.

1 Introduction

Heart diseases like myocardial infarcts are common causes of death in the western world. To find and evaluate heart defects, nuclear medicine imaging techniques such as SPECT are used. SPECT as a three-dimensional functional imaging technique may be used to show the amount of perfusion in the parts of the Left Ventricle (LV). The volume of the non-perfused tissue of the LV indicates severity of the malfunction.

To perform a quantitative perfusion analysis, it is necessary to incorporate anatomical knowledge into the functional data in terms of a segmentation of the LV. This is challenging because of the poor image quality in SPECT with its low spatial resolution and its low signal-to-noise ratio. Furthermore, clinically relevant datasets have perfusion defects at different positions of the LV. These defects are visible as low-intensity gaps in the images, but have to be included in the segmentation. Hence, we use a deformable model for segmentation that represents the shape of the LV and is registered with the SPECT data.

The deformable model contains the necessary anatomical knowledge to evaluate the relation between perfusion and anatomy. Starting from an initial shape that is positioned near to the true solution, the model is adapted to the data. We choose a surface model that represents the shape of the wall of the LV.

2 Related work

There exists a lot of literature about the segmentation of the LV in medical imaging data. However, most research has been done in the field of high resolution morphological imaging techniques like CT and MRI, as in [1–3], but only few methods exist to segment the LV in SPECT.

Data-driven segmentations of SPECT data are not sufficient, and necessary anatomical information need to be included in the method. Anatomical information may be supplemented either from a different modality (e.g. CT, MRI [4]) or using a mathematical model that describes the shape of the LV [5]. The challenge of the latter approach is to restrict geometric variation to valid LV shapes while letting the model adapt to the image data. Additionally, a smooth definition is desired as the LV is anatomically smooth.

Super ellipsoids are used to segment objects in medical imaging data [6]. Pohle et al. [5] used that method to segment the LV in 4D SPECT data. The initial position of the ellipsoid is given by a user, and to achieve a better fit to the image data, a free-form deformation is applied to the ellipsoid. Since the ellipsoid is only a coarse representation for the LV, the difference between model and data is often too large to be corrected by the subsequent free-form deformation. Furthermore, the method does not account for loss of signal in the ventricular wall due to perfusion defects.

Dornheim et al. [7] solved the segmentation problem in SPECT using a spring-mass model (SMM) that defines the anatomic shape of the LV and is registered to the functional image data. Sensors guide the spring-mass-model through the process. The surface nodes are attracted to the wall of the LV in terms of high intensity gradients while additional internal mesh nodes sample high intensity values. The results are promising, but the segmentation is neither very accurate nor smooth.

*cmh@isg.cs.uni-magdeburg.de

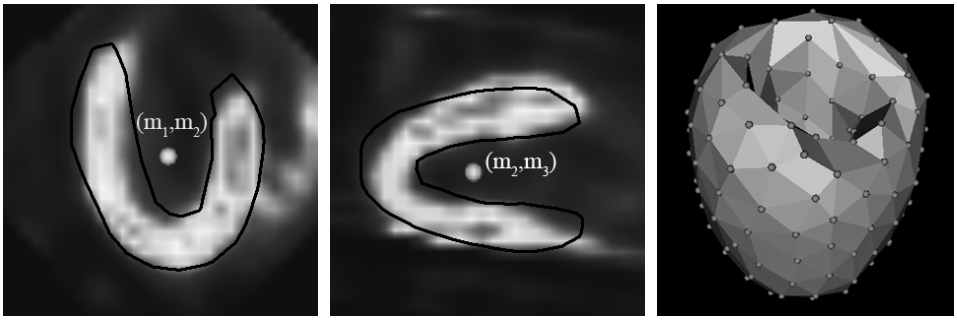

(a) XY-slice (b) YZ-slice (c)

Figure 1: The shape prototype is initialised by choosing the midpoint (m_1, m_2, m_3) from two different views 1(a) and 1(b). In 1(c) the 3D model is displayed.

3 Method

Our method is based on a shape prototype of the LV that is iteratively adapted to patient-specific data. This is complicated because the patient-related variation of the shape of the LV is quite large and the prototype needs to be fitted to the data in the presence of noise. Furthermore, due to the low spatial resolution the ventricular wall is only a few voxels thick. The challenge is to integrate the necessary shape variation in the method while keeping the method robust with respect to imaging artefacts.

Our strategy is first to let the user roughly position the prototype in the data and then adapt the LV boundary locally. Hence, we define a model of the boundary of the LV represented as a triangular mesh $P = \{(p_1, p_2, p_3)\}$, where each triangle is defined by its node positions $\mathbf{x}(p_i)$. The size of each triangle roughly equals the spatial resolution of the SPECT data. For LV detection the user selects a prototype P_j out of four existing prototypes which represent the LV with thin/thick walls and of different size (small, large). The midpoint (m_1, m_2, m_3) of the model is then registered to the image data by choosing a point in the data that corresponds to the midpoint (Fig. 1). Afterwards, the LV is approximately registered with the image data. We then propose a fine-tuning step to adapt the model to the image data and subsequently compute an exact segmentation of the LV. The fine-tuning incorporates local shape variation of the user-positioned model.

Our method employs an Active Surface (AS) [8] to represent the shape of the LV boundary. The AS is a three-dimensional extension of the traditional active contour approach by [9]. Shape variation is governed by internal and external forces. The internal forces ensure smoothness of the model reflecting the assumed smoothness of the LV boundary. External forces guide the model to image features. Given a good initialisation, the model should then deform into local image features. In case of a well-perfused LV local boundary features (i.e. the gradient) should be reliable enough. Even if a part of the LV is underperfused, this adaptation should still happen since the partial volume effect will cause the signal in this part to be higher than the background signal. The internal forces of the AS should be strong enough to counteract adverse influences from noise and other artefacts.

The AS is implemented by a dynamic FEM similar to [8] of which its elements are given by P represent the LV boundary (Fig. 1), i.e. the model M_{LV} consists of n finite elements e: $M_{LV} = \cup_{i=1}^{n} e_i$, where $e_i = (p_{i,1}, p_{i,2}, p_{i,2})$, $p_i \in P$.

The model deformation is obtained by solving the Lagrangian equations of motion,

$$\mathbf{M}\ddot{\mathbf{u}}(t) + \mathbf{C}\dot{\mathbf{u}}(t) + \mathbf{K}\mathbf{u}(t) = \mathbf{f}(t), \tag{1}$$

where $\mathbf{M}$ denotes the constant mass matrix, $\mathbf{C}$ denotes the damping matrix, $\mathbf{K}$ is the stiffness matrix and $\mathbf{f}$ is a vector of external forces. The vector $\mathbf{u}$ describes the displacement for each node. In our case, Rayleigh damping is used for $\mathbf{C}$, and $\mathbf{K}$ is a function of elastic parameters which are set by the user.

External forces shall attract the nodes to relevant object features in the image. As in non-pathological cases the LV is represented in the image data as a connected, goblet-shaped entity, whose intensity is higher than the background, high intensity gradients indicate the boundary of the LV. The image-based external forces $\mathbf{f_{ext}}(t)$ are defined such that they drag the model nodes p_i towards high intensity gradients: $\mathbf{f_{ext}}(t) = \delta \nabla I(p_i)$, $\delta > 0$, where ∇ denotes the gradient and $I(p_i)$ the intensity of the voxel corresponding to p_i.

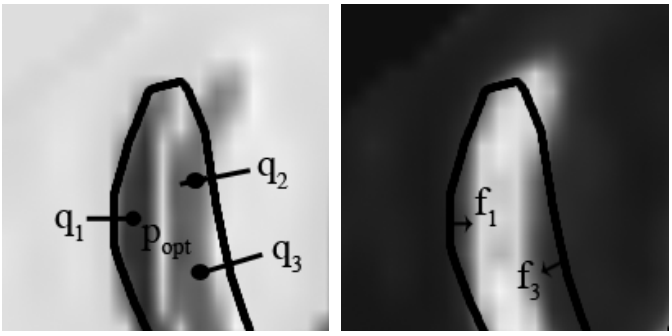

(a) (b)

Figure 2: Schematic illustration of the external forces. 2(a) shows the section of an intensity gradient image with search vectors $\mathbf{q_1}$, $\mathbf{q_2}$ and $\mathbf{q_3}$. On $\mathbf{q_i}$, high gradients magnitudes are searched. 2(b) shows the resulting force vector $\mathbf{f_1}$ and $\mathbf{f_3}$ in the section of an intensity image. Note that the force vector corresponding to $\mathbf{q_2}$ is too short to be displayed.

In our case, the search for high intensity gradients is constrained, i.e. only strong gradients in close proximity to the current position p_i are considered. Furthermore, the direction of the current surface normal and the attracting gradient must be similar. As the initial position of the model is assumed to be close to the true LV boundary, the initial relationship between surface normal and gradient direction should be retained throughout the deformation process.

Therefore, the external forces are not directly derived from the intensity gradient at the nodal position. Instead, the external forces are computed as spring forces which attract the current nodal position $\mathbf{x}(p_i)$ to a nearby optimal position $\mathbf{x}(p_{opt})$. The direction $\mathbf{q}$, in which p_{opt} is searched, is constrained by the unit normal $\mathbf{n}$ of the triangular element that contains the node p_i. The search vector $\mathbf{q}$ is defined through the points $q_s = p_i - \beta\, \mathbf{n}(p_i)$ and $q_e = p_i + \beta\, \mathbf{n}(p_i)$. β is defined so that $|\mathbf{q}| = 2\,\gamma\,s$, where s denotes the pixel spacing of the image and γ determines the length of the search vector $\mathbf{q}$ (Fig. 2). The norm of the vector $\mathbf{q}$ is then γ voxels. The optimal model point position is then $p_{opt} = p_j,\ j = \max_{p_j \in q} |\nabla I(p_j)|^2$, where $|\nabla I|^2$ denotes the gradient magnitude. To compute the intensity gradient, trilinear interpolation is employed. The external forces are

$$\mathbf{f_{ext}}(p_0) = \lambda(\mathbf{x}(p_{opt}) - \mathbf{x}(p_i)), \lambda > 0. \tag{2}$$

The motion of a node is further constrained by the sign of the gradient. If $sgn(\nabla I(p_i)) \neq sgn(\nabla I(p_{opt}))$, the node p_{opt} is neglected and no force acts on this node. This shall prevent an adaption to the wrong side of the wall.

If external forces $\mathbf{f} = \mathbf{f_{ext}}$ are known, equation (1) is solved using numerical integration [10].

The iterative deformation process stops if node displacement of all nodes goes below a predefined minimum.

The LV wall may not be found automatically because the initial position of the model is too far from the true LV boundary. This often happens if a defect is located in the upper parts of the LV, where the wall of the LV does not coincide with high intensity gradients. In these cases, the segmentation process may be supported by user interaction. The user can add attracting points as interactive forces $\mathbf{f_{user}}$ similar to [9], which incorporate a user-defined spring force. A combined force vector $\mathbf{f_c}$ on each node then replaces $\mathbf{f}$ in equation (1): $\mathbf{f_c} = \mathbf{f_{ext}} + \alpha \cdot \mathbf{f_{user}}$, where $\alpha > 0$ denotes the strength of the user-defined forces.

4 Results

We tested our method on nine SPECT datasets containing the LV. The datasets contained both healthy and pathological cases. Datasets 1-3 were obtained from a heart phantom [11], datasets 4-9 contained patient data. All datasets had an in-slice resolution of 128 x 128 pixels and 60 to 128 slices. The isotropic pixel spacing was 4.4 mm and 4.8 mm, respectively. The images were reoriented as it is the standard procedure to analyse nuclear medicine images. Reorientation rotates the dataset in such a way that the main axis of the heart is always parallel to the Y-axis in the data. Manual segmentation provided by a medical physicist, who is experienced in the field of heart quantification, was used as gold standard. For segmentation, the user was asked to select the most appropriate prototype from the list of 4 available models and to place the model into the data.

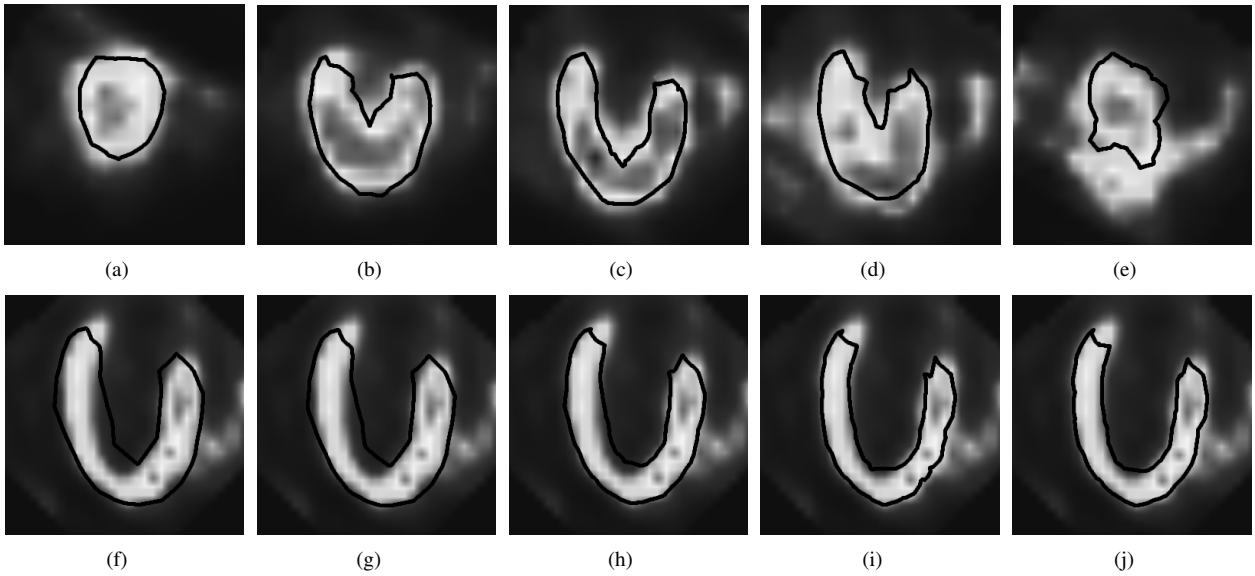

(a) (b) (c) (d) (e)

(f) (g) (h) (i) (j)

Figure 3: Segmentation results. First row: segmentation of a small LV with an appropriate model. Different slices are shown. Second row: visualisation of the segmentation process of a long LV with thin wall.

We experimentally found the following parameter values for computing the segmentation: $\gamma \in [1, 3]$, $\lambda \in [50, 200]$ (equation (2)). A value of $\alpha = 2$ has been chosen to emphasise the interactive forces.

The quality of our segmentations was examined in comparison with the gold standard segmentations (G). We computed:

- the *Jaccard coefficient* that measures the voxel-wise overlap between segment S and G: $\delta_J = \frac{|S \cap G|}{|S \cup G|}$.
- the *mean contour distance* between the boundaries b_S and b_G of S and G, measured in voxels: $\delta_{MC} = \frac{\sum_{s \in b_S} \min_{g \in b_G}(d(s,g)) + \sum_{g \in b_G} \min_{s \in b_S}(d(g,s))}{|b_S| + |b_G|}$, where $d(a, b) = |a - b|^2$.
- the *statistical relevance* that evaluates the ratio between the amount of total voxels $N_{tp} \in G$ and the amount of falsely classified voxels $N_{fp} \in S$: $\delta_R = \frac{N_{tp}}{N_{tp} + N_{fp}}$.

Our approach leads to similar results as the gold standard segmentation (Table 1). Given the appropriate prototype P, the segmentation was successful in all cases independent from the shape of the LV and possible perfusion defects (see Fig. 3 for example).

Results were also compared with results from the automatic segmentation method [7] (Table 1). In all cases, the difference was significant ($p < 0.05$). As expected, our method leads not only to a visual smooth segmentation result but also to a better fit to the image data compared with the SMM.

Results of our method depend on the initial position of the AS, because it provides a local optimisation. If the shape of the prototypes are too different from the LV in the patient data, our software allows for a scaling of the model in x/y/z direction. All user interaction is very simple, and in most cases only placements by choosing a point (m_1, m_2) in a slice (m_3) of the dataset is required.

Our method is designed such that the original shape is retained while it adapts to the LV boundary, the user is responsible to choose a model that represents the shape characteristics of the LV in the current image data. Strong shape constraints are required to ensure that the model does not adapt to irrelevant nearby objects in the SPECT images.

We tested the segmentation method on a standard PC (1.86 GHz dual core CPU with NVidia GeForce graphics card). The total computation time differs between 1 and 5 minutes which is considerably faster than a manual segmentation (between 15 and 21 minutes, as reported in [7]), and allows for user interaction to be incorporated into the segmentation process.

method	measure	1	2	3	4	5	6	7	8	9
AS	δ_J	0.78	0.84	0.79	0.75	0.79	0.72	0.70	0.79	0.67
	δ_{MC}	0.19	0.20	0.22	0.21	0.30	0.20	0.21	0.23	0.42
	δ_R	0.90	0.89	0.86	0.89	0.84	0.86	0.89	0.89	0.77
SMM	δ_J	0.69	0.75	0.74	0.72	0.65	0.62	0.62	0.74	0.63
	δ_{MC}	0.34	0.27	0.25	0.18	0.51	0.34	0.38	0.26	0.43
	δ_R	0.84	0.84	0.84	0.88	0.75	0.76	0.80	0.87	0.74

Table 1: Evaluation of segmentations of 9 test datasets using our method (AS) with respect to the gold standard. Analysis of results from [7] (SMM) are shown for direct comparison.

The robustness of the method with respect to changes of parameters has also been tested. We found that changes up to 20 % of each of the parameters did not lead to deterioration of the results.

5 Conclusion

We introduced a novel approach that aims at correct and reproducible segmentations of the LV in SPECT images. While its global shape is modelled by a prototypical initial surface, our algorithm computes a fine-tuning segmentation to adapt the model locally to the boundary of the LV in the image. The model represents the anatomy of the LV which is important since we are dealing with functional image data that has low spatial resolution and is corrupted by noise and artefacts. By choosing this approach, we ensured a certain global shape and also found a locally optimal deformation of the shape model. Perfusion defects are included in the segmentation while smoothness constraints are incorporated into the FEM. Our algorithm uses external forces which drive the deformation of the surface model to adapt to the boundary of the LV in terms of reliable intensity gradient magnitudes. Experimental results proved the efficiency and adequacy of the method. However, the fine-tuning segmentation process is dependent on the initial model position. Thus, we implemented easy to use tools for interactive positioning and scaling of the model according to the image data.

Acknowledgements

We would like to thank the Medical Imaging Research Group (MIRG) of the UBC, Vancouver for providing the data and manual segmentations, and for collaboration. This work is partially funded by the LSA (FKZ: 5161AD/0308M).

References

1. L. Cohen. "On active contour models and balloons." *CVGIP: Image Understanding* **53(2)**, pp. 211–218, 1991.
2. M. Kaus, J. Berg, J. Weese et al. "Automated segmentation of the left ventricle in cardiac MRI." *Medical Image Analysis* **8(3)**, pp. 245–254, 2004.
3. G. Hamarneh & T. Gustavsson. "Combining snakes and active shape models for segmenting the humanleft ventricle in echocardiographic images." *Computers in Cardiology 2000* pp. 115–118, 2000.
4. H. Nakajo, S. Kumita, K. Cho et al. "Three-dimensional registration of myocardial perfusion SPECT and CT coronary angiography." *Ann Nucl Med* **19(3)**, pp. 207–15, 2005.
5. R. Pohle, M. Wegner, K. Rink et al. "Segmentation of the left ventricle in 4d-dSPECT data using free form deformation of super quadrics." In *Proc. of SPIE Vol*, volume 5370, pp. 1388–1394. 2004.
6. E. Bardinet, L. Cohen & N. Ayache. "Tracking and motion analysis of the left ventricle with deformable superquadrics." *Medical Image Analysis* **1(2)**, pp. 129–149, 1996.
7. L. Dornheim, K. Tönnies & K. Dixon. "Automatic Segmentation of the Left Ventricle in 3D SPECT Data by Registration with a Dynamic Anatomic Model." *Lecture Notes in Computer Science* **3749**, pp. 335, 2005.
8. L. Cohen & I. Cohen. "Finite-element methods for active contour models and balloons for 2-D and 3-D images." *Pattern Analysis and Machine Intelligence, IEEE Transactions on* **15(11)**, pp. 1131–1147, 1993.
9. M. Kass, A. Witkin & D. Terzopoulos. "Snakes: Active contour models." *International Journal of Computer Vision* **1(4)**, pp. 321–331, 1988.
10. T. J. R. Hughes. *The finite element method: linear static and dynamic finite element analysis*. Dover Pub., Mineola, NY, 2000.
11. W. Segars et al. *Development and application of the new dynamic NURBS-based cardiac-torso (NCAT) phantom*. University of North Carolina at Chapel Hill, 2001.